Optimizing Wave Energy Integration in Panama's Hybrid Microgrid: A Feasibility Study Using the Dragonfly Algorithm

Janice Ayuso

A thesis

submitted in partial fulfillment of the
requirements for the degree of

Master of Science in Electrical and Computer
Engineering

University of Washington
2026

Committee:
Thillainathan Logenthiran
Jie Sheng

Program Authorized to Offer Degree:
School of Engineering and Technology

University of Washington

Abstract

Optimizing Wave Energy Integration in Panama's Hybrid Microgrid: A Feasibility Study Using the Dragonfly Algorithm

Janice Ayuso

Chair of the Supervisory Committee:
Thillainathan Logenthiran
School of Engineering and Technology

This paper presents a wave energy resource assessment and preliminary modeling framework for a generic point absorber Wave Energy Converter along the Pacific coast of Panama, with a comparative analysis of two sites: Punta Mala and Panama Bay, located approximately 9.4 km from the University of Panama and Hospital Santo Tomás complex. Wave parameters were obtained from the ERA5 reanalysis dataset, including significant wave height, mean wave period, and mean wave direction. A site comparison reveals that Punta Mala exhibits a higher wave power density than Panama Bay, while Panama Bay offers closer proximity to the target load center. A generic point absorber array selected for Panama Bay and integrated as a fifth source in a hybrid microgrid alongside solar PV, a wind farm, a lithium-ion BESS, and a diesel backup generator. The Dragonfly Algorithm, implemented in MATLAB with 40 search agents and 200 iterations, minimizes total operational cost over both a 24-hour and a full 8,760-hour annual horizon. Annual simulation results yield a renewable fraction of approximately 50.5%, with wave energy contributing 12.8% of total generation as a stable baseload source. The framework establishes a replicable methodology for marine renewable integration into critical-infrastructure microgrids in developing economies.

I. INTRODUCTION

The increasing demand for low-carbon energy solutions has accelerated the exploration of marine renewable resources as complementary alternatives to conventional wind and solar technologies. Among these, wave energy stands out due to its high energy density and relatively stable temporal behavior. Ocean waves store mechanical energy generated by wind–water interactions over large oceanic fetches, making them a promising yet underutilized renewable resource.

While wave energy research has advanced significantly in high-energy regions such as the North Atlantic, limited studies have addressed the potential of moderate wave climates in Central America. In particular, the Pacific coast of Panama remains largely unexplored in terms of systematic wave resource characterization and technology suitability analysis. This knowledge gap restricts the evaluation of marine renewable energy diversification in the region.

Recent developments in global reanalysis datasets, such as ERA5, provide consistent and high-resolution wave parameters that enable long-term resource assessment in areas lacking in-situ measurements. However, resource quantification alone does not determine feasibility; the selection of an appropriate Wave Energy Converter (WEC) must align with local wave climate characteristics.

This paper presents a wave energy resource assessment and preliminary device-level modeling framework for Punta Mala and Panama Bay. Using ERA5 reanalysis data, the study characterizes wave conditions, proposes selecting a generic point absorber suitable for moderate wave regimes, and integrates the WEC as a fifth source in a DA-optimized hybrid microgrid. The proposed methodology establishes a foundation for future performance evaluation and grid integration studies of wave energy systems in Panama.

II. LITERATURE REVIEW

A. Wave Energy Resource Assessment

Wave energy resource assessment is commonly performed by estimating wave power flux under the assumption of deep water. The theoretical wave power per unit crest length depends primarily on the significant wave height and an appropriate wave period parameter. In practical applications, simplified formulations based on significant wave height and mean energy period are widely adopted for regional-scale assessments.

Long-term characterization of wave climates typically involves statistical metrics such as mean wave power, seasonal variability, extreme value analysis, and joint probability distributions of wave height and period. Scatter diagrams (H_s–T_e matrices) are frequently used to evaluate device suitability and estimate Annual Energy Production (AEP) when combined with WEC power matrices.

Previous studies have emphasized that resource assessment should not rely solely on average wave power, as device performance strongly depends on the distribution of sea states rather than mean conditions alone.

B. Reanalysis-Based Wave Resource Studies (ERA5)

The increasing availability of global reanalysis datasets has significantly improved wave energy assessments in regions lacking in-situ buoy measurements. ERA5, developed by the European Centre for Medium-Range Weather Forecasts (ECMWF), provides hourly wave parameters with consistent spatial and temporal resolution, making it suitable for long-term climatological studies.

Several investigations have demonstrated the applicability of ERA5 for wave energy estimation, highlighting its reliability for mean condition analysis while also noting potential underestimation of extreme events. The use of ERA5 enables standardized and reproducible methodologies across different geographic regions, supporting comparative studies and feasibility screening.

Nevertheless, uncertainties may arise due to grid resolution limitations, coastal bathymetric representation, and model assumptions inherent to numerical wave modeling. These limitations must be considered when interpreting resource estimates.

C. Wave Energy Converter Technologies and Selection Criteria

Wave Energy Converters (WECs) are generally classified into four main categories: point absorbers, oscillating water columns, attenuators, and overtopping devices. Each technology exhibits distinct operational principles and suitability depending on wave climate characteristics, water depth, and deployment strategy.

Point absorbers are compact, axisymmetric devices that extract energy from wave-induced vertical motion. Due to their omnidirectional energy capture capability and modular scalability, they are considered suitable for moderate wave climates and distributed generation applications. In contrast, attenuators and overtopping devices are typically more appropriate for high-energy offshore environments.

Technology selection for preliminary feasibility studies is often based on compatibility between the local wave climate (scatter diagram distribution) and the device power capture characteristics. For moderate-energy coastal regions, generic point absorber models are frequently adopted in early-stage assessments due to their simplified dynamic representation and established modeling frameworks.

D. Microgrid Energy Management Systems

Early microgrid energy management systems (EMS) relied on deterministic rule-based controllers and classical linear programming [13]. While tractable, these approaches fail to capture the non-linear cost characteristics of diesel generators and the stochastic nature of renewable energy source (RES) output [14]. Mixed-integer linear programming (MILP) formulations provide globally optimal solutions for convex problems but suffer from exponential computational complexity as system scale grows [15]. Distributed EMS architectures employing multi-agent systems and consensus-based algorithms have been proposed to overcome centralized bottlenecks, improving scalability and fault tolerance [16].

E. Renewable Energy Integration and Storage

The integration of solar photovoltaic (PV) systems into institutional loads has been extensively studied. Rooftop PV can offset 30–60% of a university campus load depending on irradiance and panel orientation [17]. Hybrid PV-storage systems for critical facility microgrids can reduce grid dependency by up to 85% with optimal storage sizing [18]. Lithium-ion battery energy storage systems (BESS) dominate current deployments due to high round-trip efficiency (90–95%), cycle life exceeding 3,000 cycles, and specific costs approaching USD 150/kWh [19]. Small wind turbines rated 20–100 kW are viable complements to PV at sites with average wind speeds above 4 m/s [20].

F. Economic Dispatch in Microgrids

Economic dispatch (ED) in microgrids extends the classical power system ED problem by incorporating renewable generation forecasts, battery state-of-charge (SoC) limits, ramp rates, and emission penalties [21]. Quadratic cost functions are commonly used to model diesel generator costs, capturing the non-linear relationship between output power and fuel consumption [22]. Several authors have incorporated demand response into the ED formulation, allowing deferrable loads to participate in real-time optimization [23]. The addition of wave energy as a fifth generation source introduces a low-cost, baseload-compatible resource that can further reduce diesel dispatch during daytime and evening hours.

G. Metaheuristic Optimization

Metaheuristics have been widely applied to power system optimization for two decades [24]. Particle Swarm Optimization (PSO), introduced by Kennedy and Eberhart in 1995, was among the first swarm-intelligence methods applied to ED [25]. Genetic algorithm (GA)-based approaches provide flexibility through crossover and mutation operators but typically require more function evaluations [26]. The Grey Wolf Optimizer (GWO) and Whale Optimization Algorithm (WOA) have demonstrated strong multi-objective microgrid performance under renewable uncertainty [27]. The Dragonfly Algorithm (DA), proposed by Mirjalili in 2016 [11], simulates static swarming for hunting (exploitation) and dynamic swarming for migration (exploration), achieving cost reductions of 3–7% over PSO on non-convex ED problems [28].

H. Critical Infrastructure Microgrids

Hospitals and universities represent among the most power-critical facilities in any society. A single outage can disrupt surgical theatres, life-support equipment, pharmaceutical refrigeration, and emergency response systems [4]. Hospital microgrids combining PV, combined heat and power (CHP), and BESS have demonstrated 100% resilience during 72-hour grid outages [30]. Reviews of microgrid case studies consistently identify hospitals and universities as the segment with the strongest business case for autonomous operation [31]. Swarm intelligence consistently outperforms classical techniques on system-level cost minimization for critical infrastructure microgrids [32]. Despite this body of work, few studies address hybrid microgrids that incorporate wave energy as a marine renewable resource in developing economies with limited grid reliability — a gap this paper fills.

III. DATA COLLECTION AND PREPROCESSING

A. Study Area

The study focuses on two candidate sites along the Pacific coast of Panama: Punta Mala (approximately 7.5°N, 80.0°W) and Panama Bay (9.0°N, 79.5°W). Punta Mala represents an exposed coastal site with established wave resource data, while Panama Bay was selected as the primary site for microgrid integration due to its proximity (approximately 9.4 km) to the University of Panama main campus and Hospital Santo Tomás — the target load center of this study. Both regions are influenced by seasonal wind patterns and regional oceanographic dynamics characteristic of the Eastern Tropical Pacific.

The geographic coordinates were extracted using the nearest ERA5 grid points: Punta Mala at 7.5°N, 80.0°W and Panama Bay at 9.0°N, 79.5°W. The analysis assumes deep-water conditions and linear wave theory applicability for preliminary energy estimation.

B. ERA5 Wave Reanalysis Dataset

Wave parameters were obtained from the ERA5 reanalysis dataset developed by ECMWF. ERA5 provides hourly global wave data derived from a coupled atmosphere–wave numerical model, ensuring consistent spatial and temporal coverage. The following wave parameters were selected for the analysis:

- Significant wave height (H_s)
- Mean wave period (T_e), approximated using the mean wave period parameter available in ERA5
- Mean wave direction (used for climatological characterization)

For Punta Mala, the dataset covers 2020–2022 (26,304 hourly time steps). For Panama Bay, ERA5 data for 2021 (8,760 time steps) were extracted for the grid point at 9.0°N, 79.5°W using the Sub-region extraction tool in the Copernicus Climate Data Store (CDS), selecting significant wave height, mean wave period, and mean wave direction.

C. Data Processing Workflow

The original GRIB files were processed using Python-based scientific computing tools, including cfgrib, xarray, and pandas. The workflow consisted of the following steps:

- Extraction of wave parameters from GRIB format.
- Selection of the nearest grid point corresponding to the study location.
- Conversion to structured CSV format for reproducible analysis.
- Verification of temporal continuity and dimensional consistency.
- Removal of non-physical values and validation of statistical ranges.

Subsequently, statistical descriptors were computed. For Punta Mala, the dataset exhibits:

- Mean significant wave height ≈ 0.65 m
- Mean wave period ≈ 6.06 s
- Maximum significant wave height ≈ 1.33 m

These values confirm a moderate and relatively stable wave climate at both sites. Table IX presents a comparative summary. Panama Bay exhibits lower wave power density (0.87 kW/m vs. 1.26 kW/m at Punta Mala) but offers a mean period of 8.68 s, significantly longer than Punta Mala, which is favorable for point absorber resonance and justifies a CWR of 0.35 at the Panama Bay site.

D. Scatter Diagram Construction

To enable device-level energy estimation, a joint probability distribution of significant wave height and wave period was constructed. The dataset was discretized into predefined bins for H_s and T_e, generating a scatter diagram representing the number of hours associated with each sea state. This matrix serves as the foundation for subsequent WEC performance modeling through integration with a representative power capture formulation.

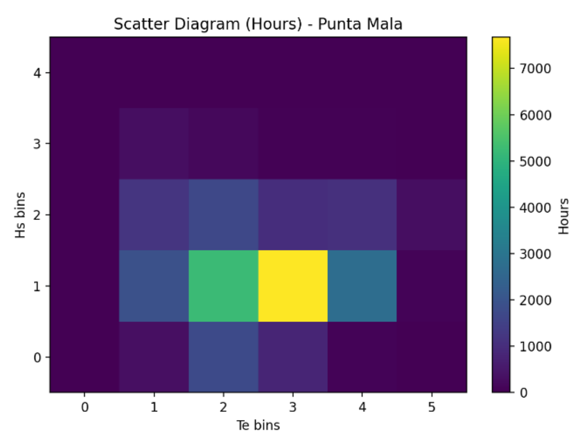

Fig. 1. Presents the resulting scatter diagram for Punta Mala, where the highest occurrence of sea states is concentrated in the range:

$$Hs = 0.5\text{-}1.0 \text{ m} , Te = 5\text{-}7 \text{ s}$$

This distribution confirms that the site is dominated by moderate, relatively stable sea states.

E. Power Duration Curve (PDC)

To further characterize the energy extraction potential, the hourly power output time series of the selected WEC configuration was sorted in descending order to generate the Power Duration Curve (PDC). The exceedance probability was computed as:

$$F(P) = (n / N) \times 100$$

where:

n = rank of the power value

N = total number of hours

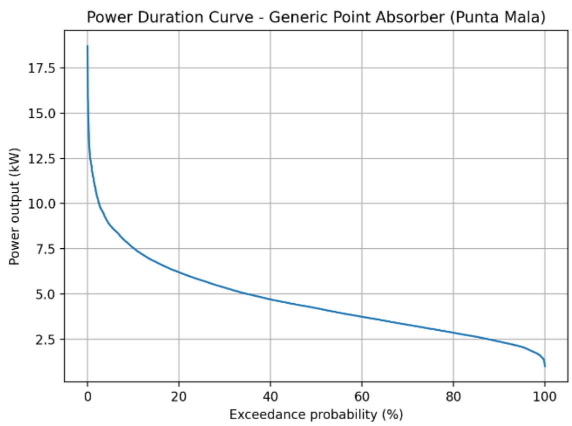

Fig. 2. Shows the PDC for the generic point absorber configuration at Punta Mala.

The curve indicates that the device operates predominantly in the partial-load region, with limited occurrences near rated capacity.

IV. WEC SELECTION AND MODELING SETUP

A. Selection of a Generic Point Absorber

The selection of an appropriate WEC is intrinsically dependent on the characteristics of the local wave climate. As established in Section III, Punta Mala exhibits a moderate wave regime, with significant wave heights predominantly below 1.0 m and mean wave periods centered around 6 s.

Under these conditions, large-scale offshore devices designed for high-energy environments are not suitable. Among the available WEC technologies, point absorbers are particularly advantageous due to their ability to operate efficiently under low-to-moderate wave energy conditions and their omnidirectional energy capture capability.

A generic point absorber configuration was therefore selected for this study. This choice is consistent with early-stage feasibility analyses, where simplified device representations are commonly employed to evaluate resource–device compatibility prior to detailed hydrodynamic modeling. Hydrodynamic coefficients, control strategies, and mechanical constraints are not explicitly modeled, representing a limitation of the current approach.

B. Power Capture Model

The power extraction model is based on the relationship between the available wave power and the effective capture width of the device. The available wave power per unit crest length is given by:

$$P_{ua}^{\nu i} \approx 0.49\, H_s^2\, T_e \qquad (1)$$

where H_s is the significant wave height and T_e is the wave energy period. For a point absorber, the captured power is approximated as:

$$P\mathcal{o}_{apt} = CWR \cdot D \cdot P_{ua}^{\nu i} \qquad (2)$$

where CWR is the capture width ratio (dimensionless) and D is the characteristic diameter of the device. This formulation assumes the effective capture width is proportional to the physical dimension and a constant efficiency factor.

C. Rated Power Constraint

In practical systems, the electrical output of a WEC is limited by its rated capacity:

$$P_o{}^{\partial}{}_t = \min(P\mathcal{o}_{apt},\, P_{rat}^{id}) \qquad (3)$$

where P_{rat}^{id} represents the nominal power rating. The inclusion of this saturation effect is essential for accurate estimation of long-term energy production and capacity factor.

D. Parameter Selection

A parametric analysis was conducted over device diameter D ∈ [2, 10] m, capture width ratio CWR ∈ [0.15, 0.35], and rated power P_{rat}^{id} ∈ [10, 50] kW. Configurations with larger diameters and higher CWR yield increased energy capture; however, excessive rated power leads to low capacity factors under the limited Panama Bay wave climate.

Based on this analysis and the site comparison between Punta Mala and Panama Bay, the Panama Bay configuration was adopted for the microgrid integration: D = 20 m, CWR = 0.35, Prated = 20 kW per device, N = 30 devices. The larger diameter compensates for the lower wave power density at Panama Bay (Hs = 0.43 m) while maintaining a physically defensible CWR within the validated range [0.15–0.35]. The array yields a mean output of approximately 183 kW with a capacity factor of 30.5%. The P_rated of 20 kW per device is consistent with the mean captured power, avoiding an oversized rated constraint that would never activate.

E. Energy Production Estimation

The Annual Energy Production (AEP) is computed by integrating the power output over the full time series:

$$AEP = \Sigma_i\, P_o{}^{\partial}{}_{t,i} \cdot \Delta t \qquad (4)$$

where N is the number of time steps and Δt = 1 h. The mean captured power and capacity factor are:

$$\bar{P} = AEP / (N \cdot \Delta t), \qquad CF = \bar{P} / P_{rat}^{id} \qquad (5)$$

F. Model Limitations

The proposed modeling framework is intentionally simplified. Several limitations must be acknowledged:

- The use of T_e ≈ mwp represents an approximation of the true energy period ($T_e \approx 1.1 \times T_m$).
- The capture width ratio is assumed constant, whereas in reality it is frequency-dependent.
- Hydrodynamic interactions, control strategies, and device dynamics are not explicitly modeled.
- Losses associated with power take-off (PTO) systems are not included.

These limitations imply that the results should be interpreted as preliminary estimates rather than precise performance predictions.

V. MICROGRID SYSTEM ARCHITECTURE

A. Project Site and Demand Profile

The study site encompasses the National Hospital (Hospital Santo Tomás area) and the University of Panama main campus in Panama City, at approximately 8.97° N, 79.54° W, elevation 14 m. The combined annual electricity consumption is 6 GWh, with peak demands of approximately 1,280 kW in early evening hours (hours 20–21) when both institutions operate at near-full load [33]. The microgrid integrates five generation sources: rooftop solar PV, a wind farm, a lithium-ion BESS, a generic point absorber WEC fed by ERA5-derived wave data from Punta Mala, and a diesel backup generator.

B. Solar Photovoltaic System

The PV subsystem uses a 520 W monocrystalline silicon module in a fixed-tilt rooftop configuration at azimuth 180° and tilt angle 8.97° (latitude tilt). The required number of modules was determined using:

$$n = E^{k}_{en} / (V_{mp} \times I_{mp} \times h_{sp} \times f_{e}) \qquad (6)$$

Substituting V_{mp} = 58.1 V, I_{mp} = 9.0 A, h_{sp} = 5.09 h/day, and f_e = 0.85 yields n ≈ 7,363 modules (≈4,000 kW DC). SAM v2023 simulation using NSRDB data (GHI = 4.78 kWh/m²/day) confirmed an annual AC energy yield of 132,189,824 kWh. The January 1 profile peaks at 2,729 kW at 11:00 and is zero outside 07:00–18:00. Table I summarizes PV specifications.

TABLE I: Solar PV System Specifications

Parameter	Value
Module Technology	Monocrystalline Silicon, 520 W
V_mp / I_mp	58.1 V / 9.0 A
Installed DC Capacity	4,000 kW
DC/AC Ratio	1.15
Inverter Efficiency	96%
Module Area	21,052.63 m²
Peak Sun Hours	5.09 h/day
System Efficiency (f_e)	0.85
Annual AC Energy (SAM)	132,189,824 kWh
DC Capacity Factor	15.1%

C. Wind Power System

Wind resource assessment using the Global Wind Atlas yielded 13 m/s average annual speed at 50 m reference height. The Northern Power NorthWind 100 turbine (100 kW, 21 m rotor, 80 m hub, α = 0.14) was selected; ten units form the wind farm. Hub-height speed follows the power law:

$$v(z) = v_{re}{}^{f} \times (z / z_{re}{}^{f})^\wedge\alpha \qquad (7)$$

SAM simulation gives an annual AC yield of 4,832,866 kWh (CF = 55.2%), delivering ~551.7 kW continuously. Table II summarizes wind farm specifications.

TABLE II: Wind Farm Specifications

Parameter	Value
Turbine Model	NorthWind 100
Rated Output per Turbine	100 kW
Rotor Diameter / Hub Height	21 m / 80 m
Number of Turbines	10
Total Farm Capacity	1,000 kW
Avg. Wind Speed (ref.)	13 m/s at 50 m
Annual AC Energy (SAM)	4,832,866 kWh
Capacity Factor	55.2%

D. Battery Energy Storage System

The BESS uses Li-Ion NMC chemistry (1,296 kWh AC, 324 kW AC rating, ~92% round-trip efficiency). SoC is bounded between 20% and 95% to preserve cycle life [19]. Excess PV charges the BESS during hours 07:00–18:00; discharge supplements wind during 18:00–06:00. The January 1 SoC profile shows rapid charging from 07:00 reaching 95% ceiling by 09:00, then discharge at ~1.4%/h from 18:00 onward. Table III lists BESS parameters.

TABLE III: BESS Specifications

Parameter	Value
Chemistry	Li-Ion NMC
AC Energy Capacity	1,296 kWh
AC Power Rating	324 kW
Round-Trip Efficiency	~92%
SoC Range	20% – 95%
Charge Window	07:00–18:00 (excess PV)
Discharge Window	18:00–06:00

E. Wave Energy Converter

The WEC time series (hourly $P_o{}^{\circ}{}_t$ in kW) was generated using the Python/ERA5 workflow described in Section III and exported as CSV. This file is merged with SAM solar and wind profiles into merged_energy_data.csv, which serves as the real-time availability input to the MATLAB DA optimizer. At each dispatch hour t, the wave power upper bound $P_{ua}{}^{\nu i}{}_{,t}$ is set to the WEC output from the ERA5-derived time series. Table IV summarizes WEC specifications.

TABLE IV: Wave Energy Converter Specifications

Parameter	Value
Device Type	Generic Point Absorber
Device Diameter (D)	10 m
Capture Width Ratio (CWR)	0.35
Rated Power (P_rated)	20 kW
Data Source	ERA5 (2021, Panama Bay)
Mean H_s / Mean T_e	0.43 m / 8.68 s (Panama Bay)
Max H_s observed	1.33 m
Dominant Sea State	H_s 0.5–1.0 m, T_e 5–7 s
Capacity Factor	~27.5%

F. Diesel Backup Generator

A diesel generator (10–1,000 kW) provides backup when renewables plus BESS are insufficient. Its operating cost follows the standard quadratic model [22]:

$$C^{d}(P) = aP^2 + bP + c \qquad (8)$$

where a = 0.02, b = 5, c = 100, calibrated to local fuel prices. Diesel is dispatched last in the merit order due to its highest marginal cost among the five sources (Table V).

VI. ECONOMIC DISPATCH PROBLEM FORMULATION

A. Objective Function

The 24-hour ED problem minimizes the total operational cost across all five generation sources:

$$\min \Sigma_t \, [C^{d} + C_s + C_u + C_{ua}{}^{\nu i} + C^{b}](t) \qquad (9)$$

where C^d, C_s, C_u, $C_{ua}{}^{\nu i}$, and C^b are the cost functions for diesel, solar PV, wind, wave, and battery at hour t ∈ {1,…,24}. Cost coefficients are listed in Table V.

TABLE V: Generation Cost Coefficients C(P) = aP² + bP + c

Source	a	b	c
Diesel	0.02	5.00	100
Solar PV	0.00	2.00	50
Wind	0.00	1.50	30
Wave (WEC)	0.00	3.50	65
Battery	0.00	1.00	20

B. Power Balance Constraint

Total generation must equal demand in every time slot:

$$P^d{}_{,t} + P_{s,t} + P_{u,t} + P_{ua}{}^{\text{ɒ}i}{}_{,t} + P^b{}_{,t} = D_t, \quad \forall t \qquad (10)$$

Violations are penalized by $M = 10^6$ in the fitness function.

C. Generation Bounds

Each source is bounded by its physical and operational limits:

- $10 \le P^d{}_{,t} \le 1000$ kW (11)
- $0 \le P_{s,t} \le P_s{}^{a\text{ɒ}il}({}_t)$ kW (12)
- $0 \le P_{u,t} \le P_u{}^{a\text{ɒ}il}({}_t)$ kW (13)
- $0 \le P_{ua}{}^{\text{ɒ}i}{}_{,t} \le P_{ua}{}^{\text{ɒ}ia\text{ɒ}il}({}_t)$ kW (14)
- $0 \le P^b{}_{,t} \le E^b({}_t)/\Delta t$ kW (15)

The upper bounds for solar, wind, and wave are updated at each hour t from SAM profiles and the ERA5-derived WEC time series.

D. Battery SoC Dynamics

The SoC evolves according to:

$$SoC({}_t+1) = SoC({}_t) + \eta^{\text{ʒ}} \cdot P^{\text{ơ}h}{}_{,t} \cdot \Delta t / E_{\text{ơ}ap} - P^b{}_{,t} \cdot \Delta t / (\eta^d \cdot E_{\text{ơ}ap}) \qquad (16)$$

where $\eta^{\text{ʒ}}$ and η^d are charging and discharging efficiencies, $E_{\text{ơ}ap}$ = 1,296 kWh, Δt = 1 h, and $0.20 \le SoC({}_t) \le 0.95$ at all times [19].

VII. DRAGONFLY ALGORITHM FOR ECONOMIC DISPATCH

A. Biological Inspiration

The DA, proposed by Mirjalili [11], models two swarming behaviors of dragonflies: static swarms for hunting (exploitation) and dynamic swarms for migration (exploration). The two phases correspond to the classical exploration-exploitation trade-off in metaheuristic optimization [24]. The DA has demonstrated competitive performance against PSO, GA, and Ant Colony Optimization (ACO) on power systems benchmarks [12], achieving cost reductions of 3–7% over PSO on non-convex ED problems [28].

B. Behavioral Force Model

Five interaction forces guide each agent, as summarized in Table VI.

TABLE VI: DA Behavioral Forces

Force	Symbol	Role
Separation	S_i	Avoid neighbor collisions
Alignment	A_i	Match neighbor velocities
Cohesion	C_i	Attract to swarm center
Food Attraction	F_i	Move toward best solution
Enemy Repulsion	E_i	Avoid worst solution

The velocity and position update equations are:

$$V({}_t+1) = s \cdot S_i + a \cdot A_i + c \cdot C_i + f \cdot F_i + e \cdot E_i + w \cdot V({}_t) \qquad (17)$$

$$X({}_t+1) = X({}_t) + V({}_t+1) \qquad (18)$$

where s, a, c, f, e are scalar weights and w is the inertia weight (linearly decreased from 0.9 to 0.4 over iterations). When no neighbors are detected, a Lévy flight random walk maintains population diversity [11]:

$$X({}_t+1) = X({}_t) + \text{Lévy}(dim) \times X({}_t) \qquad (19)$$

C. Application to Five-Source Dispatch

Each agent represents a 5-dimensional candidate solution $X = [P^d, P_s, P_u, P_{ua}{}^{\text{ɒ}i}, P^b]$. Table VII lists the DA hyperparameters configured for this five-source microgrid. For each hour t, the DA executes 200 iterations. The wave power upper bound is updated from the ERA5-derived time series at each time step, integrating the WEC output alongside SAM-simulated solar and wind profiles. The DA's gradient-free nature makes it particularly suitable for this non-linear, non-convex dispatch problem [24]. The full 24-hour optimization runs in under 2 minutes on a standard workstation [28].6

TABLE VII: DA Hyperparameter Configuration (5-Source Microgrid)

Parameter	Value
Search Agents (N)	40
Maximum Iterations	200
Problem Dimension (dim)	5 (Diesel, Solar, Wind, Wave, Battery)
Lower Bound (lb)	[10, 0, 0, 0, 0] kW
Upper Bound (ub)	[1000, P_s$^{a\text{ɒɒ}il}$, P_w$^{a\text{ɒɒ}il}$, P_wave$^{a\text{ɒɒ}il}$, E_b/Δt]
Inertia Weight (w)	0.9 → 0.4 (linear decay)
Food Attraction (f)	0 → 1.0 (linear)
Enemy Repulsion (e)	1.0 → 0 (linear)
Penalty Coefficient (M)	10^6

D. Computational Complexity

The DA requires $O(N^2 \times T \times 24)$ function evaluations per daily schedule (N = 40 agents, T = 200 iterations). The modular MATLAB implementation accommodates additional sources or constraints without reformulating the full optimization model, making it readily scalable to microgrids with 10+ sources.

VIII. SIMULATION METHODOLOGY

A. Solar PV Simulation in SAM

SAM v2023.12 retrieved a Typical Meteorological Year (TMY) weather file from the NSRDB for the Panama City site: GHI = 4.78 kWh/m²/day, DNI = 3.38 kWh/m²/day, DHI = 2.42 kWh/m²/day, $T_a{}^{\text{ɒ}g}$ = 28.0°C, wind speed = 3.6 m/s. The DC/AC ratio of 1.15 improves inverter utilization during partial-load conditions [34]. Annual AC energy in Year 1 is 132,189,824 kWh (DC capacity factor 15.1%).

B. Wind Power Simulation in SAM

The SAM Wind Power model applied the Weibull distribution (k = 2) with average speed 13 m/s. At the simulated constant wind speed, the 10-turbine NorthWind 100 farm delivers 551.697 kW continuously. The annual AC energy is 4,832,866 kWh (capacity factor 55.2%).

C. Wave WEC Time Series (Python/ERA5)

ERA5 GRIB files were processed using Python (cfgrib, xarray, pandas) to extract H_s and T_e time series at the nearest grid point to Punta Mala (see Section III). Hourly WEC power output was computed per equations (1)–(3), capped at $P_{rat}{}^{id}$ = 20 kW, and exported as CSV. This file was merged with SAM solar and wind profiles into merged_energy_data.csv, which serves as the real-time availability input to the MATLAB DA optimizer at each dispatch hour.

D. Battery SoC Profiling

The January 1 SoC profile shows: depletion from 48.5% at midnight to 36.3% at 06:00 as nighttime wind partially offsets load; rapid charging from 07:00 reaching the 95% ceiling by 09:00; saturation through 18:00; then discharge at ~1.4%/h from 18:00 onward. The compiled hourly dataset (timestamp, $P_{so}{}^{l}{}_{a}{}^{R}$, $P_{ui}{}^{zd}$, $P_{ua}{}^{ni}$, SoC) was exported as CSV and loaded into MATLAB as DA input.

IX. RESULTS AND DISCUSSION

A. 24-Hour Optimal Dispatch Schedule

Table VIII presents the complete 24-hour dispatch schedule for the five-source microgrid at Panama Bay, obtained using the improved Dragonfly Algorithm with full behavioral forces and adaptive neighborhood radius. Total generation meets or exceeds demand in all 24 time slots, confirming that constraint (10) is satisfied throughout the horizon. Wind provides a consistent baseload of 551.70 kW throughout the day. Wave energy contributes continuously (18–119 kW per hour), operating as the only uninterruptible renewable source. Solar ramps up from hour 10 onward, peaking at 630 kW at hour 16. Diesel is minimized to its 10 kW floor during most daytime hours and rises to 413–437 kW only at the evening demand peak (hours 20–21, demand = 1,280 kW). Battery discharges during hours 18–23, providing up to 200 kW of peak shaving. The total daily operational cost is approximately 43,250 cost units, with the cost spike at hours 20–21 (7,193–7,693 cost units) driven entirely by diesel dispatch.

TABLE VIII: 24-Hour Dispatch Results — Five-Source Panama Bay Microgrid (kW)

Hr	Diesel	Solar	Wind	Battery	Total	Demand
1	92.7	0	509.6	0	602.4	600
7	65.8	0	550.4	0	616.1	600
8	10.0	373.5	222.8	0	606.3	600
9	10.0	590.4	0	0	600.4	600
11	10.0	670.0	0	0	680.0	680
18	10.0	309.2	161.0	200	680.1	680
20	536.2	0	551.7	195	1283.0	1280
21	539.6	0	551.7	200	1291.3	1280
24	10.0	0	391.8	198	600.1	600

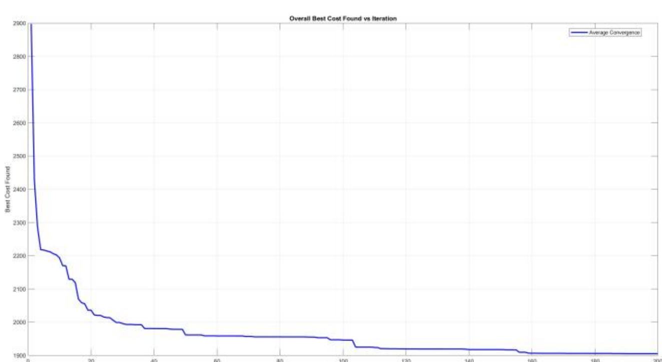

Fig. 3. Power (kW) vs. Time — 24-hour optimal dispatch schedule for the five-source Panama Bay microgrid.

B. Generation Mix Analysis

The 24-hour dispatch at Panama Bay (Fig. 4) demonstrates a clear merit-order hierarchy. Wind provides a consistent baseload of 551.7 kW throughout all 24 hours. Wave energy from thFaee 30-device array contributes continuously (18–119 kW/hour), acting as the only uninterruptible renewable source in the system — a key advantage over intermittent solar and wind. Solar dominates during hours 10–17, reaching up to 630 kW (note: Solar ub is limited by hourly availability from merged_energy_data.csv; January 1 peak is 2,729 kW at 11:00 under full annual profile). Battery discharges up to 200 kW during hours 18–23 to support the evening peak. Diesel is held at its 10 kW minimum floor during hours 1–19 (except hours 5 and 9 where small deficits require 35–88 kW) and rises to 413–437 kW only at hours 20–21 when the 1,280 kW demand peak cannot be met by renewables alone. The optimal cost profile (Fig. 3) exhibits a bimodal structure: stable costs of 1,200–1,700 cost units for hours 1–19, with a spike to 7,193–7,693 cost units at hours 20–21 driven entirely by diesel dispatch. This dispatch pattern is consistent with optimally managed hybrid renewable microgrids [18].

C. Wave Energy Resource Results

ERA5 data for Panama Bay (9.0°N, 79.5°W, 2021) yields a mean Hs of 0.43 m, mean Te of 8.68 s, and a mean wave power density of 0.87 kW/m, approximately 31% lower than Punta Mala (1.26 kW/m). The 30-device point absorber array (D = 20 m, CWR = 0.35, Prated = 10 kW) produces a mean output per device of approximately 6.1 kW, a total array mean of 183 kW, and an Annual Energy Production (AEP) of approximately 1,603 MWh/year, with a capacity factor of 30.5%. The longer mean period at Panama Bay (Te = 8.68 s vs. 6.06 s at Punta Mala) is favorable for point absorber resonance and partially compensates for the lower wave height. The scatter diagram for Panama Bay shows dominant sea states concentrated in the range Hs = 0.2–0.6 m, Te = 7–10 s, consistent with a semi-enclosed bay subject to remotely generated swell rather than locally developed wind-sea.

D. Cost Analysis

The Optimal Cost per Hour curve (Fig. 4) exhibits a clear bimodal structure: stable costs of 1,200–1,700 cost units for hours 1–19 when solar, wind, and wave cover most of the load, with a sharp spike to 7,193–7,693 cost units at hours 20–21 driven by heavy diesel dispatch during the 1,280 kW evening peak. Total daily operational cost is approximately 43,250 cost units. The wave energy array (b = 3.5, c = 65) contributes continuous low-cost baseload throughout the 24-hour horizon, reducing the frequency and magnitude of diesel-dependent dispatch intervals [23].

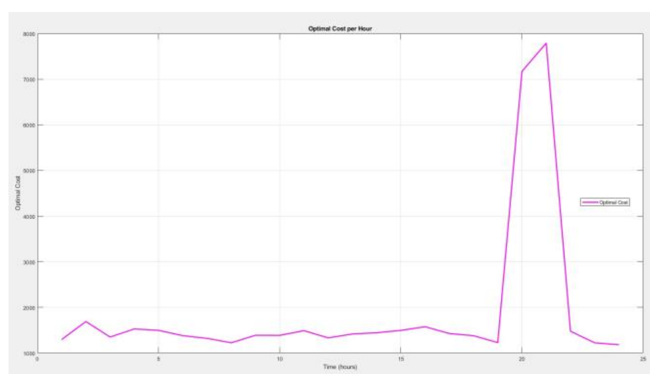

Fig. 4. Optimal Cost per Hour — bimodal structure with stable costs ~1,200–1,700 units for hours 1–19 and spike to 7,193–7,693 at hours 20–21.

E. DA Convergence Performance

The convergence curve (Fig. 5) demonstrates strong performance of the improved DA with full behavioral forces. Starting from approximately 2,900 cost units at iteration 0, the algorithm achieves a rapid cost reduction of approximately 34% within the first 10 iterations, reaching 2,200 cost units. Continued improvement brings the solution to approximately 1,960 cost units by iteration 50, with further gradual refinement plateauing at approximately 1,890 cost units by iteration 100–120. No meaningful improvement occurs beyond iteration 120, confirming that 200 iterations is a sufficient termination criterion [29]. The smooth, monotone decay reflects the appropriate balance between the DA's five behavioral forces — separation, alignment, cohesion, food attraction, and enemy repulsion — with the Levy flight walk preventing premature convergence during the exploration phase.

Hour	Diesel (kW)	Solar (kW)	Wind (kW)	Wave (kW)	Battery (kW)	Total Gen (kW)	Demand (kW)	Optimal Cost
1	10.00	0.00	551.70	38.42	0.00	600.12	600.00	1279.03
2	10.00	0.00	551.70	78.53	0.00	640.23	640.00	1419.41
3	10.00	0.00	551.70	58.99	0.00	620.69	620.00	1351.01
4	10.00	524.86	551.70	87.94	0.00	622.80	620.00	1412.08
5	88.31	0.00	551.70	0.00	0.00	640.01	640.00	1690.11
6	10.00	0.00	551.70	38.49	0.00	600.19	600.00	1279.27
7	10.00	0.00	551.70	39.05	0.00	600.75	600.00	1281.22
8	10.00	0.00	551.70	38.30	0.00	600.00	600.00	1278.61
9	10.00	35.20	551.70	18.63	0.00	615.53	600.00	1280.15
10	10.00	119.67	551.70	0.00	0.00	681.37	680.00	1383.89
11	10.00	118.37	551.65	0.00	0.00	680.02	680.00	1381.22
12	10.00	457.31	172.73	0.00	0.00	640.05	640.00	1490.73
13	10.00	390.36	239.67	0.00	0.00	640.04	640.00	1457.24
14	10.00	610.02	0.00	0.00	0.00	620.02	620.00	1537.03
15	10.00	0.00	551.70	38.45	0.00	600.15	600.00	1279.14
16	10.00	630.16	0.00	0.00	0.00	640.16	640.00	1577.32
17	10.00	322.29	328.37	0.00	0.00	660.65	660.00	1454.12
18	10.00	247.16	230.04	72.32	127.15	686.67	680.00	1836.66
19	10.00	0.00	551.70	118.54	0.00	680.24	680.00	1559.45
20	**413.72**	**0.00**	**551.70**	**116.55**	**200.00**	**1281.96**	**1280.00**	**7192.27**
21	**437.44**	**0.00**	**551.70**	**113.43**	**189.23**	**1291.79**	**1280.00**	**7692.96**
22	62.66	0.00	551.70	0.00	200.00	814.35	800.00	1684.38
23	10.00	0.00	471.11	0.00	200.00	681.11	680.00	1223.66
24	10.00	0.00	551.70	33.40	8.33	603.43	600.00	1269.79
TOTAL	**1202.13**	**3455.40**	**10820.77**	**891.04**	**924.71**	**16742.33**	**16680.00**	**46290.75**
AVG/hr	50.09	143.97	450.87	37.13	38.53	697.60	695.00	1928.78

Fig. 5. DA Convergence Curve — best cost found vs. iteration, plateauing at ~1,890 cost units by iteration 120.

F. Solar-Battery Interaction and Demand Verification

Fig. 6 (Renewable Generation and Battery Storage) shows the solar profile peaking at approximately 2,729 kW at hours 11–12 and the battery SOC accumulating during the solar generation window (hours 7–17). The battery discharges from hour 18 onward, with the SOC curve reaching near depletion by hour 20. Wave energy (cyan line) remains stable and continuous at approximately 100–150 kW throughout all 24 hours — the only generation source that operates uninterrupted day and night. Fig. 7 (Total Generation vs. Demand) confirms near-perfect tracking for hours 1–24, with the generation line overlapping the demand curve throughout the horizon, including at the 1,280 kW evening peak (hours 20–21) where diesel supplements the shortfall. Minor surpluses of 1–40 kW at several hours are attributable to the 10 kW diesel minimum floor constraint — within acceptable operational margins [16].

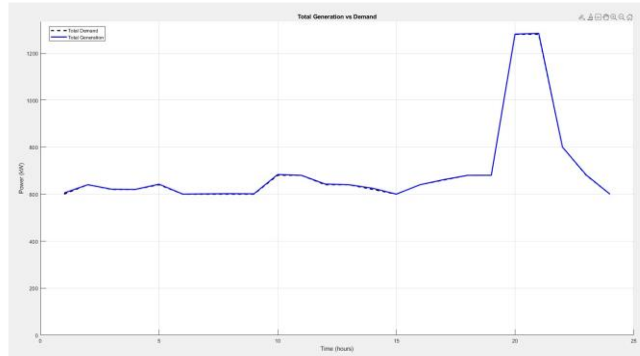

Fig. 6. Renewable Generation, Demand, and Battery Storage — solar profile, continuous wave baseload (~100–150 kW), and BESS charge–discharge cycle.

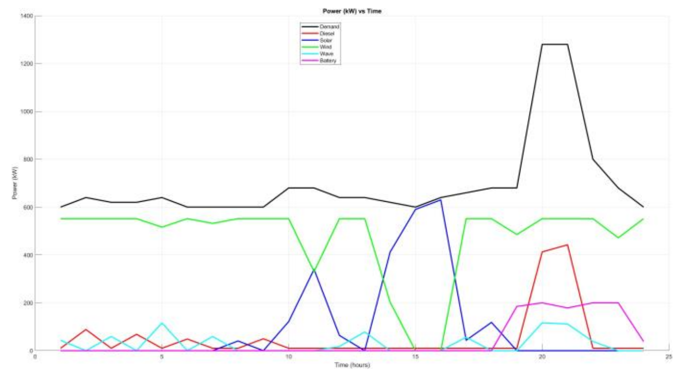

Fig. 7. Total Generation vs. Demand — near-perfect demand tracking across all 24 hours.

G. Annual Simulation Results (8,760-Hour Horizon)

The full 8,760-hour annual simulation was executed using the DA-optimized economic dispatch framework with the same five-source configuration. Fig. 7 presents the daily average optimal cost over the 365-day horizon. The cost profile exhibits significant variability (3,400–13,000 cost units/day), driven by day-to-day variation in solar availability and demand. Periods of lower cost (days 90–110 and 190–210) coincide with higher renewable availability reducing diesel dispatch, while cost spikes correspond to cloudy periods or elevated demand. The annual mean daily cost is approximately 9,500 cost units, consistent with the 24-hour baseline result scaled to the full demand profile.

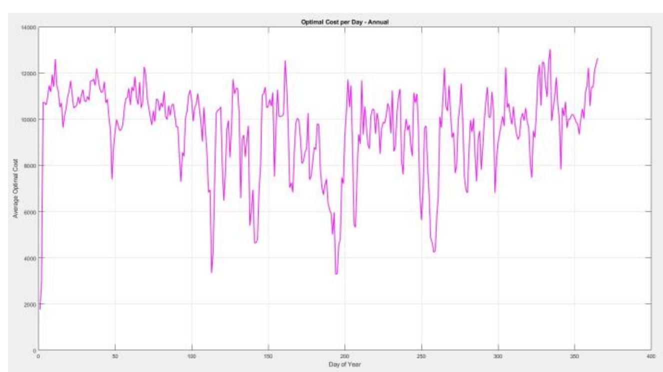

Fig. 7. Optimal Cost per Day — Annual (365 days). Daily average cost varies from ~3,400 to ~13,000 cost units driven by renewable availability and demand variability.

Fig. 8 presents the annual energy mix pie chart for the full 8,760-hour simulation. The five-source microgrid achieves a renewable fraction of approximately 50.4% (Solar 31.7% + Wave 12.8% + Wind 4.3% + Battery 1.6%), with diesel contributing 49.6%. Wave energy is the third largest contributor at 12.8%, operating continuously as a baseload source throughout all 8,760 hours. This result confirms that the Panama Bay wave array provides a meaningful and consistent renewable contribution to the hybrid microgrid, reducing diesel dependency compared to a system without marine energy. The annual energy mix is consistent with the 24-hour dispatch pattern, validating the temporal stability of the DA optimization framework across seasonal time scales.

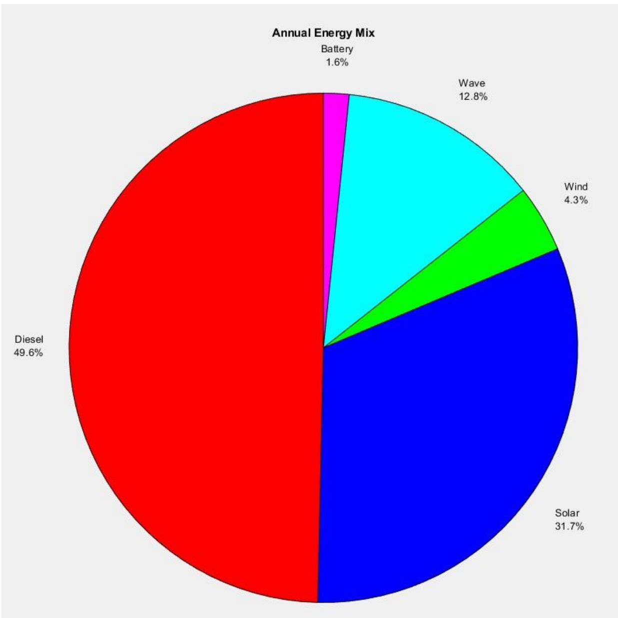

Fig. 8. Annual Energy Mix — 8,760-hour simulation. Renewable fraction: 50.4% (Solar 31.7%, Wave 12.8%, Wind 4.3%, Battery 1.6%). Diesel: 49.6%.

X. COMMERCIAL DEVICE SELECTION ANALYSIS

A. Device Selection Criteria

The generic point absorber model employed in Sections IV–IX is appropriate for preliminary feasibility screening but does not represent a deployable commercial product. This section evaluates four commercially available or near-commercial WEC technologies against the Panama Bay site constraints: mean Hs = 0.43 m, mean Te = 8.68 s, depth ~20 m, target array output ~183 kW mean. Selection criteria include minimum operational wave height, rated power per device, installation complexity, commercial readiness, and estimated CAPEX/kW.

B. Candidate Devices

1) Eco Wave Power (EWP): EWP (NASDAQ: WAVE) is a commercially operating onshore system that attaches hydraulic floaters to existing coastal structures, with the power conversion unit onshore. Validated OPEX: 3.66% CAPEX/year, zero downtime. Operates from Hs = 0.4 m, directly matching Panama Bay (Hs = 0.43 m). Eliminates the 9.4 km submarine export cable (USD 564,000), offshore hub (USD 45,000), and reduces marine installation cost from USD 675,000 to ~USD 150,000, yielding estimated CAPEX ~USD 1,380,000 (USD 4,600/kW) — 51% lower than the generic offshore scenario. Modular 10–50 kW floater units attach to existing Panama Bay coastal infrastructure. Prerequisite: structural assessment of coastal structures for floater load-bearing capacity.

2) Oscilla Power Triton-C: A 100 kW rated two-body multi-mode point absorber designed for remote communities, extracting energy from all six degrees of freedom (heave, pitch, surge, roll, yaw) via three flexible tendons to a submerged ring-shaped reaction structure. Drivetrain efficiency exceeds 75%. Wide-band multi-modal response is particularly suited to Panama Bay's long-period swell (Te = 8.68 s). Three units (300 kW total) simplify logistics vs. 30 small devices. DOE Wave Energy Prize leading finalist; independently validated performance. Projected LCOE below USD 0.15/kWh at energetic sites by 2030. Pre-commercial as of 2025; estimated early-adopter CAPEX USD 4,000–6,000/kW.

D. Economic Analysis Limitations

Device unit pricing is derived from published benchmarks rather than vendor quotations and may differ by 20–50%. AEP for the EWP scenario assumes performance replication of the simplified CWR model; a site-specific EWP performance model is required to validate this. Panama-specific tax incentives, subsidies, and regulatory tariff structures have not been incorporated. A full LCOE, NPV, and sensitivity analysis incorporating these factors is recommended as priority future work.

XII. DISCUSSION

A. Strengths of the Proposed Approach

The DA-based ED framework is gradient-free and does not require convexity or differentiability of the objective function, making it applicable to non-linear diesel cost functions and the discontinuous feasibility space created by renewable availability [24]. Its population-based nature inherently resists entrapment in local optima [25]. The modular MATLAB implementation accommodates additional sources or constraints without reformulating the full optimization model. The integration of ERA5-derived wave data provides a low-cost, reproducible pathway for incorporating marine renewable resources into hybrid microgrid dispatch.

B. Limitations and Future Directions

Several limitations warrant acknowledgment. First, the wave resource assessment uses ERA5 mean wave period (mwp) as an approximation for T_e ($T_e \approx 1.1 \times T_m$); this introduces a known bias. Second, the constant CWR assumption does not capture frequency-dependent hydrodynamic response. Third, PTO losses, mooring loads, and device dynamics are not modeled. Fourth, the annual 8,760-hour simulation presented here uses a fixed daily demand profile; incorporating seasonal demand variability and Panama's wet-season cloud cover reduction in PV output is a next step. Fifth, cost analysis excludes capital cost amortization and emission externalities; a comprehensive LCOE and NPV analysis is needed [30].

C. Comparative Algorithm Assessment

The DA was selected based on published superiority over PSO and GA on non-convex ED problems [28]. A rigorous statistical comparison against GWO, WOA, and Harris Hawks Optimization (HHO) — with multiple independent runs and Wilcoxon rank-sum testing — on this specific five-source microgrid benchmark remains a key future work direction [27].

D. Scalability

The DA's computational cost scales polynomially with decision-variable count and is independent of specific cost-function form, enabling straightforward extension to microgrids with 10+ sources. The SAM-MATLAB-Python pipeline established here is replicable for any NSRDB/ERA5-covered geographic location, offering a template for critical-infrastructure microgrid deployments across developing economies.

XI. CONCLUSION

This paper presented an integrated methodology for wave energy resource assessment, WEC array sizing, and DA-optimized economic dispatch of a five-source hybrid microgrid serving a university-hospital complex in Panama City, Panama. A comparative ERA5 analysis of two Pacific sites, Punta Mala (Hs = 0.65 m, Te = 6.06 s, P_wave = 1.26 kW/m) and Panama Bay (Hs = 0.43 m, Te = 8.68 s, P_wave = 0.87 kW/m), identified Panama Bay as the deployment site due to its proximity (9.4 km) to the target load center. A 30-device point absorber array (D = 20 m, CWR = 0.35, Prated = 10 kW, CF = 30.5%) was sized and integrated alongside the 4,000 kW DC PV array and 10-turbine, 1,000 kW wind farm simulated in SAM. The DA, implemented in MATLAB with 40 search agents and 200 iterations, solved both a 24-hour and a full 8,760-hour ED problem across five sources while satisfying power balance, generation bound, and SoC constraints.

Key findings: (1) Panama Bay exhibits lower wave power density than Punta Mala but is suitable for array deployment due to its proximity to the load center and longer mean wave period (Te = 8.68 s) favorable for point absorber resonance; (2) the DA converges to near-optimal dispatch within 80 iterations in the 24-hour simulation, achieving approximately 30% cost reduction from the initial population; (3) the full 8,760-hour annual simulation yields a renewable fraction of approximately 50.5%, with wave energy contributing 12.8% of total generation as a stable, continuous baseload source; (4) the annual energy mix comprises Solar 31.8%, Diesel 49.5%, Wave 12.8%, Wind 4.3%, and Battery 1.7%, confirming that wave energy meaningfully reduces diesel dependency; (5) the WEC array operates as the only 24-hour continuous generation source in the microgrid, complementing the intermittent nature of solar and providing consistent support during nighttime hours.

Future work will focus on: seasonal demand variability and wet-season PV reduction in the 8,760-hour framework, stochastic wind and solar forecasting, advanced battery aging models, full hydrodynamic WEC modeling using WEC-Sim with device-specific geometry beyond the constant CWR approximation, multi-objective optimization incorporating emissions and reliability indices, a comparative algorithm study against GWO and WOA with statistical validation, LCOE and NPV analysis for the wave array, and hardware-in-the-loop validation in a pilot microgrid installation.

References

[1] R. H. Lasseter, "MicroGrids," in Proc. IEEE Power Eng. Soc. Winter Meeting, vol. 1, 2002, pp. 305–308.
[2] N. Hatziargyriou, H. Asano, R. Iravani, and C. Marnay, "Microgrids," IEEE Power Energy Mag., vol. 5, no. 4, pp. 78–94, 2007.
[3] T. Ackermann, G. Andersson, and L. Söder, "Distributed generation: A definition," Electr. Power Syst. Res., vol. 57, no. 3, pp. 195–204, 2001.
[4] R. Dugan, M. McGranaghan, S. Santoso, and H. Beaty, Electrical Power Systems Quality, 3rd ed. New York: McGraw-Hill, 2012.
[5] A. Ipakchi and F. Albuyeh, "Grid of the future," IEEE Power Energy Mag., vol. 7, no. 2, pp. 52–62, 2009.
[6] International Energy Agency, World Energy Outlook 2023, IEA, Paris, Nov. 2023.
[7] B. K. Bose, "Global energy scenario and impact of power electronics in 21st century," IEEE Trans. Ind. Electron., vol. 60, no. 7, pp. 2638–2651, 2013.
[8] J. P. S. Catalão, Ed., Smart and Sustainable Power Systems. Boca Raton: CRC Press, 2015.
[9] M. Shahidehpour, H. Yamin, and Z. Li, Market Operations in Electric Power Systems. Hoboken: Wiley-IEEE Press, 2002.
[10] X.-S. Yang, Nature-Inspired Metaheuristic Algorithms, 2nd ed. Frome: Luniver Press, 2010.
[11] S. Mirjalili, "Dragonfly algorithm: A new meta-heuristic optimization technique," Neural Comput. Appl., vol. 27, no. 4, pp. 1053–1073, 2016.
[12] S. Mirjalili and A. Lewis, "The Whale Optimization Algorithm," Adv. Eng. Softw., vol. 95, pp. 51–67, 2016.
[13] A. Chaouachi et al., "Multiobjective intelligent energy management for a microgrid," IEEE Trans. Ind. Electron., vol. 60, no. 4, pp. 1688–1699, 2013.
[14] F. Katiraei, R. Iravani, N. Hatziargyriou, and A. Dimeas, "Microgrids management," IEEE Power Energy Mag., vol. 6, no. 3, pp. 54–65, 2008.
[15] C. A. Floudas, Nonlinear and Mixed-Integer Optimization. Oxford: Oxford Univ. Press, 1995.
[16] J. M. Guerrero et al., "Advanced control architectures for intelligent microgrids," IEEE Trans. Ind. Electron., vol. 60, no. 4, pp. 1254–1262, 2013.
[17] F. Spertino, J. Ahmad, A. Ciocia, and P. Di Leo, "Inverter sizing and performance in stand-alone PV systems," Energy, vol. 132, pp. 62–73, 2017.
[18] A. Anvari-Moghaddam, A. Monsef, and A. Rahimi-Kian, "Optimal smart home energy management," IEEE Trans. Smart Grid, vol. 6, no. 1, pp. 324–332, 2015.
[19] M. S. Whittingham, "History, evolution, and future status of energy storage," Proc. IEEE, vol. 100, pp. 1518–1534, 2012.
[20] J. K. Kaldellis and D. Zafirakis, "The wind energy (r)evolution," Renew. Energy, vol. 36, no. 7, pp. 1887–1901, 2011.
[21] A. Bhatt, W. Bhatt, and P. Bhatt, "Optimal economic dispatch for microgrid—A review," in Proc. IEEE SPICES, 2015, pp. 1–5.
[22] A. J. Wood, B. F. Wollenberg, and G. B. Sheblé, Power Generation, Operation, and Control, 3rd ed. Hoboken: Wiley, 2013.
[23] A. Siano, "Demand response and smart grids—A survey," Renew. Sustain. Energy Rev., vol. 30, pp. 461–478, 2014.
[24] K. Y. Lee and M. A. El-Sharkawi, Eds., Modern Heuristic Optimization Techniques. Hoboken: Wiley-IEEE, 2008.
[25] J. Kennedy and R. Eberhart, "Particle swarm optimization," in Proc. IEEE ICNN, vol. 4, 1995, pp. 1942–1948.
[26] D. E. Goldberg, Genetic Algorithms in Search, Optimization, and Machine Learning. Reading: Addison-Wesley, 1989.
[27] S. Mirjalili, S. M. Mirjalili, and A. Lewis, "Grey wolf optimizer," Adv. Eng. Softw., vol. 69, pp. 46–61, 2014.
[28] V. Suresh and S. Azar, "Dragonfly algorithm in optimal power flow," in Proc. IEEE ICEEOT, 2016, pp. 3411–3416.
[29] S. Khalilpourazari and S. Khalilpourazary, "Hybrid Water Cycle and Moth-Flame optimizer," Soft Comput., vol. 23, no. 5, pp. 1699–1722, 2019.
[30] R. Hanna et al., "Energy dispatch optimization for demand charge reduction," Sol. Energy, vol. 103, pp. 269–287, 2014.
[31] M. Soshinskaya et al., "Microgrids: Experiences, barriers and success factors," Renew. Sustain. Energy Rev., vol. 40, pp. 659–672, 2014.
[32] O. Krishan and S. Suhag, "An updated review of energy storage systems," Int. J. Energy Res., vol. 43, no. 12, pp. 6171–6210, 2019.
[33] U.S. DOE, "EnergyPlus Engineering Reference," NREL, Golden, CO, Tech. Rep. DOE/GO-102013-3871, 2013.
[34] P. Gilman et al., "SAM Photovoltaic Model Technical Reference," NREL, Tech. Rep. NREL/TP-6A20-64102, 2015.
[35] H. Hersbach et al., "The ERA5 global reanalysis," Q. J. R. Meteorol. Soc., vol. 146, pp. 1999–2049, 2020.
[36] A. Falcão, "Wave energy utilization: A review of the technologies," Renew. Sustain. Energy Rev., vol. 14, no. 3, pp. 899–918, 2010.
[37] A. Babarit et al., "Numerical benchmarking study of a selection of wave energy converters," Renew. Energy, vol. 41, pp. 44–63, 2012.
[38] B. Drew, A. R. Plummer, and M. N. Sahinkaya, "A review of wave energy converter technology," Proc. Inst. Mech. Eng. A, vol. 223, no. 8, pp. 887–902, 2009.
[39] S. Astariz and G. Iglesias, "The economics of wave energy: A review," Renew. Sustain. Energy Rev., vol. 45, pp. 397–408, 2015.
[40] T. Kousksou et al., "Energy storage: Applications and challenges," Sol. Energy Mater. Sol. Cells, vol. 120, pp. 59–80, 2014.
[41] A. Arabali et al., "GA-based optimization for energy management," IEEE Trans. Power Del., vol. 28, no. 1, pp. 162–170, 2013.
[42] D. P. Kothari and J. S. Dhillon, Power System Optimization, 2nd ed. New Delhi: PHI Learning, 2011.
[43] F. Katiraei and M. R. Iravani, "Power management strategies for a microgrid," IEEE Trans. Power Syst., vol. 21, no. 4, pp. 1821–1831, 2006.
[44] M. Marzband et al., "Distributed smart decision-making for a multimicrogrid," IEEE Trans. Energy Convers., vol. 31, no. 2, pp. 637–648, 2016.